Trans Indian Inst Met (2019) 72(10):2763–2772
https://doi.org/10.1007/s12666-019-01753-6

TECHNICAL PAPER

Al–Steel Joining by CMT Weld Brazing: Effect of Filler Wire Composition and Pulsing on the Interface and Mechanical Properties

Krishna P. Yagati[1] · Ravi Bathe[2] · Joydip Joardar[2] · K. V. Phaniprabhakar[2] · G. Padmanabham[2]

Received: 31 January 2019 / Accepted: 5 June 2019 / Published online: 25 June 2019

Abstract Cold metal transfer welding, a low-heat input process, was employed to weld-braze 6061-T6 aluminium alloy to galvanized interstitial free steel using Al–Si-based (4043 and 4047) filler wires in lap fillet configuration. The effects of current pulsing and filler composition on interface morphology and joint strength were investigated. Pulsing, as well as Si content in the filler, affected the interfacial intermetallic compound layer morphology and joint strength. The detailed micro-area X-ray diffraction studies of seam/steel interface revealed the presence of binary (Al–Fe type) and ternary (Al–Fe–Si type) intermetallic phases for joints made with 4043 and 4047 filler, respectively. Lap shear tests proved that joints made with 4047 filler having ternary intermetallic phases were stronger and fractured in the braze seam. However, joints made with 4043 filler having binary intermetallic phases recorded interfacial failure at lower loads than joints made with 4047 filler. Therefore, the type and morphology of the interfacial intermetallic compounds were found to influence the joint performance.

Keywords Cold metal transfer welding · Wetting · Aluminium–steel dissimilar joining · Joint strength · Intermetallics · Fracture

✉ G. Padmanabham
gp@arci.res.in

[1] Department of Metallurgical and Materials Engineering, National Institute of Technology, Durgapur, West Bengal 713209, India

[2] Center for Laser Processing of Materials, International Advanced Research Center for Powder Metallurgy and New Materials (ARCI), Balapur Post, Hyderabad 500005, India

1 Introduction

Ability to join aluminium to steel enables selective replacement of steel parts by lighter aluminium parts, consequently the possibility for weight diminution of automotive bodies [1]. Distinct joining techniques such as gas metal arc welding (GMAW) [2], gas tungsten arc welding (GTAW) [3], cold metal transfer (CMT) welding [4], TIG/MIG double-sided welding [5] laser welding/brazing [6], friction stir welding [7], ultrasonic welding [8] and clinching [9] have been reported in the literature for joining aluminium alloy to steel. However, in fusion joining, formation of brittle intermetallic compounds (IMC) at aluminium–steel interface inimically affects the joint strength [10]. Recent reports indicate that IMC layer less than 10 μm does not affect the joint strength adversely [11]. Therefore, controlling the IMC layer thickness at Al–steel interface using reduced energy fusion joining techniques like laser brazing or cold metal transfer (CMT) welding is advisable. CMT process is a modified GMAW process in which the filler wire motion is incorporated into the process control and operates in a short-circuit mode. CMT process offers the advantages of spatter-free welding, highly stable arc and extremely low energy input and therefore is suitable for thin sheet and dissimilar material joining [12]. Cao et al. [13] has reported that in CMT spot plug welding of A6061-T6 aluminium alloy to galvanized steel using 4043 filler, strength of the joint is dependent on weld area. Zhang et al. [14] studied arc characteristics, metal transfer and effect of energy input in CMT joining of 6061 aluminium alloy to galvanized steel and reported a joint strength of 96 MPa. Jacome et al. [15] studied the effect of filler wire composition on the mechanical properties of CMT weld-brazed aluminium (AW5182-H111) to DX54D steel joints and reported the joint strength of

304 MPa for the joints made with $AlSi_3Mn_1$ filler wire. Yang et al. [16] investigated the effect of gap between the plates and position of arc on joint strength and recorded improved joint strength with increase in gap. Therefore, literature is comprised of reports on effect of various parameters like current, voltage, processing speed, arc position, gap between plates, external magnetic field and filler wire composition in aluminium–steel joining and it affects their bead formation characteristics and joint strength [17, 18].

Sound aluminium–steel joints form an extremely thin layer of IMC at the interface. The variation in physical properties of aluminium and steel poses a characterization challenge in identifying these IMC phases and morphologies. Various techniques like energy-dispersive spectrometry (EDS), electron probe micro-analysis(EPMA), electron backscattered diffraction (EBSD), X-ray diffraction (XRD) and transmission electron microscopy (TEM) have been reported in the literature to achieve this objective [3, 15, 19, 20]. Jacome et al. [15] used EBSD and TEM to study the intermetallic compound formed in Al–steel butt joints made with different filler wires and reported the formation of a variety of binary and ternary intermetallic phases. Zhang et al. [21] in laser welding of 5251 aluminium alloy to automotive grade steel, using XRD, reported the presence of Al_3FeSi and Fe_4Al_{13} intermetallic compounds at the interface. Jia et al. [22] reported the formation of $Fe_2Al_5Zn_{0.4}$ using XRD in laser-welded aluminium–steel joint. Qin et al. [23] analysed the laser hybrid welded aluminium–steel joint interface using XRD and reported the presence of $FeAl_2$, Fe_2Al_5 and Fe_4Al_{13}. Murakami et al. [24] arc-brazed A1050P-H24 aluminium sheet to SPCC cold-rolled plain carbon steel using a flux cored Al–12%Si filler wire and analysed the joint interface sing EPMA and EDS and examined the fracture surface(interfacial failure) using XRD. The chemical composition obtained from EPMA and EDS shows the presence of $Al_{7.4}Fe_2Si$ intermetallic compound, and XRD analysis also confirms it. In the literature, EDS is used extensively to identify the interface intermetallic compound which is not very accurate method for phase determination. Binary (Al–Fe) and/or ternary (Al–Fe–Si) IMC may form at Al/steel interface depending on the joining process and base material composition [15]. Therefore, the fracture load and location of an aluminium–steel joint can be influenced by the type of IMC formed at the interface. Ma et al. [25] reported the effect of interfacial intermetallic phases formed on crack initiation and propagation in arc-brazed 5052 aluminium alloy to galvanized steel joints made using 4043 filler wire. Hence, limited literature is available in terms of interfacial IMC phase detection and its relevance to joint strength and failure mode.

The present study is focussed on CMT joining of 6061-T6 aluminium alloy to galvanized steel. The effects of filler wire composition and pulsing on aluminium–steel interfacial characteristics and joint properties were investigated. The aluminium–steel interface was extensively studied using micro-area X-ray diffraction (micro-XRD) technique, and IMC phases were identified. The type and morphology of IMCs were correlated with joint strength and failure mode.

2 Materials and Methods

AA6061-T6 (Al–Mg–Si) aluminium alloy sheet of 2 mm thickness and galvanized interstitial free (IF) steel sheet of 1.2 mm thickness were selected as base materials. Aluminium alloys 4043 (Al–5%Si) and 4047 (Al–12%Si) of 1.2 mm diameter were used as filler wires to join dissimilar (aluminium/steel) metals in lap configuration.

Aluminium and steel sheets were sheared to a size of 150 mm × 100 mm, and the edges of aluminium sheet were grounded, brushed using stainless steel wire brush followed by ethanol swabbing prior to brazing operation. The aluminium sheet was placed over the steel sheet with 8–10 mm overlap, the gap between the sheets was maintained at around 200 μm and a CMT arc (Trans Pulse Synergic 3200 CMT) was run along the edge of the aluminium sheet. The process was designed in such a way that the aluminium workpiece and filler wire melted and covered the un-melted steel workpiece and formed a braze-like joint. Screening experiments were performed to identify the parametric window which yielded uniform weld bead with no visible defects. The optimized list of parameters is given in Table 1. Experiments were performed in two modes, i.e. with and without pulsing of CMT. The brazed joints were sectioned using abrasive cutting machine, mounted and polished with 600, 800, 1000, 1200 grit emery papers, and followed by 9, 5, 3 and 1 μm diamond suspension. The final polishing was done using 0.05 μm colloidal silica

Table 1 Processing parameters

Parameter	Process	
	CMT	P-CMT
Standoff distance (mm)	6	6
Torch angle (°)	80–85	80–85
Argon gas flow rate (GFR, L/min)	18–20	18–20
Wire position	60% on Al side	60% on Al side
Wire feed rate (WFR, m/min)	3.5, 4	3.5, 4
Processing speed (S, m/min)	1, 1.2	1, 1.2
Current (A)	55–69	61–87
Voltage (V)	11.4–12	14.6–16.5

suspension. The specimens were then ultrasonically cleaned and chemically etched using Keller's reagent (2.5 mL HNO_3, 1.5 mL HCl, 1 mL HF in 95 mL H_2O) for microstructural analysis. The etched samples were then examined under scanning electron microscope (HITACHI 3400N) with EDS (THERMONORAR) attachment. The interfacial phase study was carried out using micro-X-ray diffractometer (Rigaku RAPID-II-D/MAX) with Cu K_∞ radiation (λ = 0.154056 nm) with a step size of 0.01° in the 2θ range of 30°–120°. The diffractometer is equipped with micro-focus rotating anode source, and it gives the focal size of ~ 10 µm diameter using a 10 µm collimator. This micro-area XRD system used a very large image plate (IP) detector, which collected a significant portion of the diffracted Debye ring patterns. Thus, even if the beam fell on a single grain or a single crystal, peaks from all the planes of the grain or crystal were clearly visible in the diffraction pattern. To study joint integrity, lap shear tests were performed with sample dimensions of 150 mm × 25 mm (length × width). The lap shear tests were carried out using INSTRON 6500R universal tensile testing machine. To understand the effect of temperature behaviour in different modes (with and without pulsing) during weld-brazing process, temperatures were recorded. During CMT weld brazing, preplaced k-type thermocouple at a depth of 0.5 mm from the bottom side of 1.2-mm-thick steel plate recorded the temperature profile.

3 Results

3.1 Thermal Transients

Figure 1 shows the thermal transients recorded during the CMT and P-CMT processes. From the figure, it is noted that under similar processing conditions, in CMT without pulsing, the peak temperature is 640 °C while in pulsed CMT process, the temperature is 685 °C (Fig. 1b). It is also evident that base material has retained heat for slightly longer time period in P-CMT than in CMT without pulsing. The superimposed current or pulsing in P-CMT process has enhanced the energy input, resulting in higher heat input and high peak temperature and consequently longer heat retention.

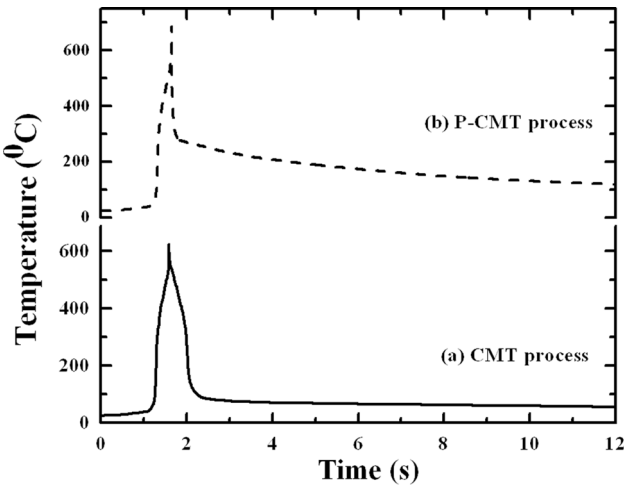

Fig. 1 Thermal profile of **a** CMT process, **b** P-CMT process

3.2 Macrostructure

Secondary electron images of transverse cross sections of aluminium–steel dissimilar joints made with CMT, P-CMT using Al–5%Si and Al–12%Si filler wire at a 4 m/min wire feed rate are shown in Fig. 2, and its bead geometry measurements are listed in Table 2. The macrostructures and the bead geometry measurements indicate that both process and filler wire composition has an effect on weld-brazing bead geometry. It is observed that under similar processing conditions, CMT weld-brazed joints made with Al–5%Si filler wire (Fig. 2a) record the bead width of 3.2 ± 0.15 mm and wetting angle of 60° ± 2°, while joints made with Al–12%Si filler wire (Fig. 2c) record a bead width of 3.8 ± 0.15 mm and wetting angle of 43° ± 2°. It is also observed that the P-CMT weld-brazed joints made with Al–5%Si filler wire (Fig. 2b) record the bead width of 3.5 ± 0.15 mm and wetting angle of 55° ± 2° and joints made with Al–12%Si filler wire (Fig. 2d) record a bead width of 4.0 ± 0.15 mm and wetting angle of 40° ± 2°. From the results, it is clearly evident that P-CMT weld-brazed joints have higher bead width and low wetting angle (an indication of improved wetting and spreading of aluminium filler melt on steel) than CMT weld-brazed joints. This may be attributed to the enhanced fluidity of aluminium melt, caused by higher peak temperature associated with the P-CMT process. It is also observed that the joints produced by CMT and P-CMT process using Al–12%Si filler (Fig. 2c, d) record low wetting angles and high bead widths than the joints made using Al–5%Si filler (Fig. 2a, b). Therefore, higher Si content in the filler wire also enhances the wetting and spreading action of the aluminium melt on steel. The addition of Si to aluminium alloys has increased the fluidity of the melt and being of eutectic composition, has resulted in improved wetting and spreading. Hence, joints made with Al–12%Si filler records higher bead width and lower wetting angle (an indication of improved wetting) compared to joints made with Al–5%Si filler. Kang et al. [26] studied the joining of A5052 aluminium to aluminized and galvanized steel using various filler wires and reported that under similar heat input conditions the galvanized steel shows better wetting and spreading compared to aluminized steel. It is also reported that in joints made with

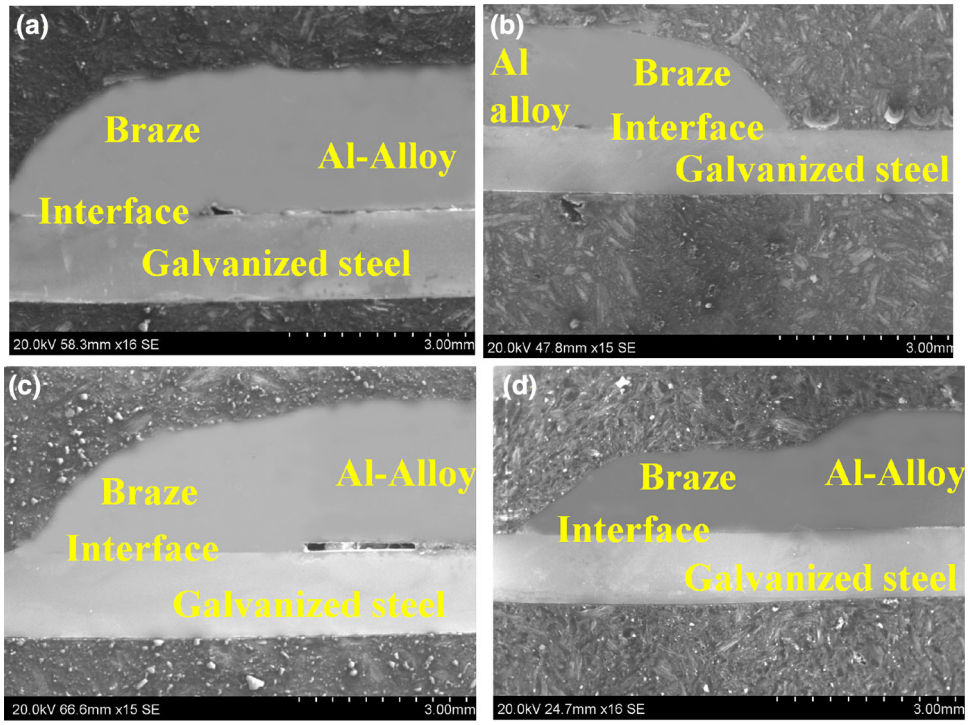

Fig. 2 Transverse cross-section SEM micrographs of aluminium/steel joints **a** CMT (Al–5%Si filler), **b** P-CMT (Al–5%Si filler), **c** CMT (Al–12%Si filler), **d** P-CMT (Al–12%Si filler)

Table 2 Bead geometry measurements

S. no	Bead geometry measurements	Range			
		Al–5%Si		Al–12%Si	
		CMT	P-CMT	CMT	P-CMT
1	Bead width (mm)	3.2 ± 0.15	3.5 ± 0.15	3.8 ± 0.15	4.0 ± 0.15
2	Bead height (mm)	1.8 ± 0.15	1.7 ± 0.15	1.6 ± 0.15	1.6 ± 0.15
3	Wetting angle (°)	60 ± 2	55 ± 2	43 ± 2	40 ± 2

galvanized steel, use of 4047 filler wire shows better wetting and spreading behaviour which agrees well with the present result analysis.

3.3 Microstructures

Figure 3a illustrates the schematic diagram of weld-brazed aluminium–steel joint in lap configuration, showing different locations of microstructural observation, i.e., Al/bead interface, braze bead and bead/steel interface. From Fig. 3b, it can be observed that the Al/bead interface is comprised of larger grains compared to braze bead and parent metal indicating the grain growth at heat affected zone (HAZ) on aluminium side. However, braze bead (Fig. 3c) shows dendritic structure indicating the solidified microstructure in all processing conditions. It is noticed that bead/steel interface (Fig. 3d) is comprised of the reaction product of aluminium melt and solid steel and varies in thickness and morphology throughout the cross section. This can be attributed to the varied thermal history of different regions caused by the intensity of the arc.

Figures 4 and 5 depict the secondary electron images of various locations of bead/steel interface obtained at 2000 × magnification, and the respective IMC layer thickness is listed in Table 3. The bead/steel interface reveals the presence of IMC layer formed due to the reaction between aluminium melt and solid steel, and its thickness is found to be restricted to less than 8 μm (permissible limit) at all processing conditions. It is also observed that the IMC layer varies in thickness and morphology throughout the cross section and the IMC layer grows thicker at a central region (Figs. 4b, e and 5b, d) compared to head (Figs. 4a, d and 5a, d) and foot (Figs. 4c, f and 5c, f) regions. This may be attributed to the high heat intensity experienced by the central region causing thickening of IMC layer. Similarly, Jacome et al. [15] and Krishna et al. [17] also reported the

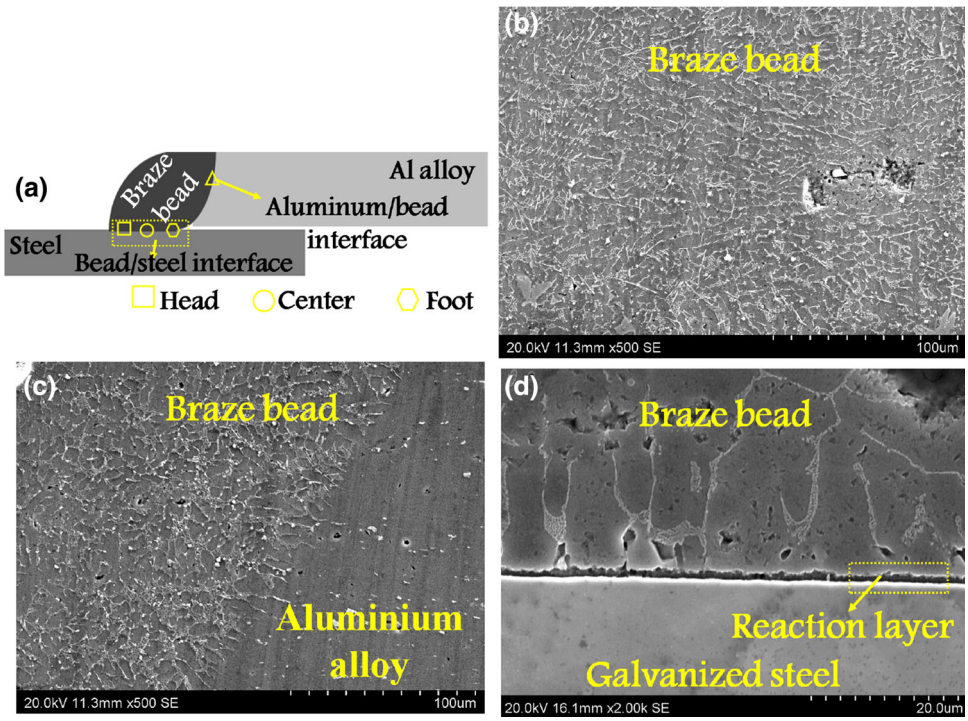

Fig. 3 SEM micrographs of the aluminium–steel joint **a** schematic indicating different regions of microstructural observation, **b** braze bead (braze zone), **c** aluminium/bead interface, **d** bead/steel interface

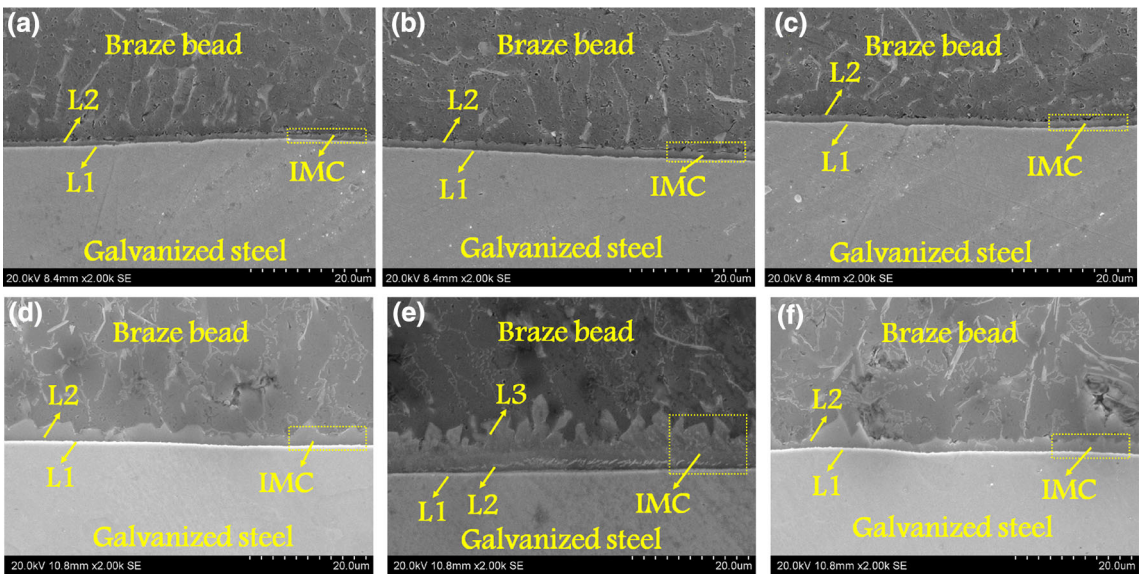

Fig. 4 SEM micrographs of various locations of seam/steel interface made with Al–5%Si filler wire at 2k magnification: **a** head (CMT), **b** centre (CMT), **c** foot (CMT), **d** head (P-CMT), **e** centre (P-CMT), **f** foot (P-CMT)

thickening of IMC layer at the central region in their respective works on CMT brazing and P-GMAW brazing of aluminium alloy to steel.

3.3.1 Effect of Pulsing

The interfacial microstructures reveals that P-CMT joints (Figs. 4d–f and 5d–f) record thicker IMC layer than CMT joints (Figs. 4a–c and 5a–c). High heat input involved in P-CMT process may probably result in thicker IMC layer.

3.3.2 Effect of Filler Wire Composition

It is observed that under similar processing conditions, joints made using Al–12%Si filler (Fig. 5) records thicker IMC layer than joints made using Al–5%Si filler (Fig. 4a–

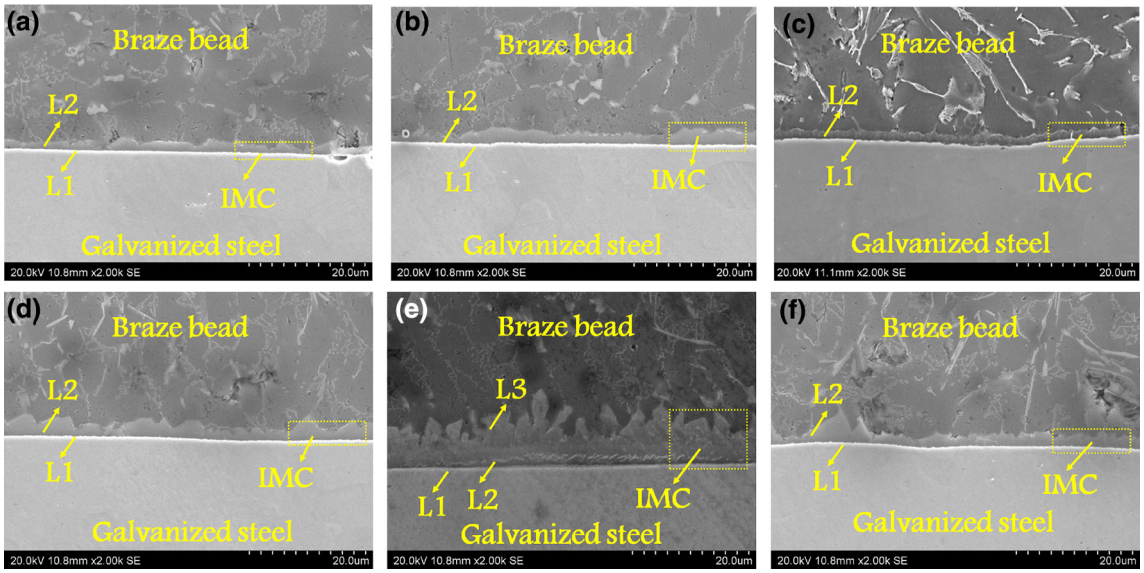

Fig. 5 SEM micrographs of various locations of bead/steel interface made with Al–12%Si filler wire at 2k magnification **a** head (CMT), **b** centre (CMT), **c** foot (CMT), **d** head (P-CMT), **e** centre (P-CMT), **f** foot (P-CMT)

Table 3 IMC layer thickness under various conditions

S. no	Location	IMC layer thickness (μm)			
		Al–5%Si		Al–12%Si	
		CMT	P-CMT	CMT	P-CMT
1	Head	1.2 ± 0.1	1.9 ± 0.1	1.2 ± 0.1	2.4 ± 0.1
2	Centre	1.6 ± 0.1	3.2 ± 0.1	3.5 ± 0.1	8 ± 0.1
3	Foot	1 ± 0.1	1.4 ± 0.1	1.6 ± 0.1	1.2 ± 0.1

e). This is because Al–12%Si being eutectic composition ($T_m \sim 577$ °C) remains in the liquid state for slightly longer time period than Al–5%Si ($T_m \sim 600$ °C) which may enhance the diffusion rate and lead to thickening of IMC layer. In the literature, it has been reported that IMC layer thickness reduces with the addition of Si to the filler wire. As a contrary, the present microstructural investigation records an increase in IMC layer thickness with an increment in Si content from 5 to 12% in the filler. This can be elucidated as follows. Fe_2Al_5 IMC phase has been predominantly reported in the literature related to hot-dip aluminizing of steel, diffusion studies of Fe and Al and in aluminium–steel joining [27–29]. Heuman et al. [30], from XRD study, divulged that the availability of more number of vacancies in c-axis of Fe_2Al_5 promotes its growth and therefore increases its thickness. However, the addition of Si hinders Fe_2Al_5 growth by occupying the vacant site in c-axis and therefore the IMC thickness reduces [31]. Hence, the mechanism indicates that addition of Si inhibits the growth of Fe_2Al_5 phase. But, in the present study, in subsequent section of phase analysis, no Fe_2Al_5 is detected. Therefore, no Fe_2Al_5 and hence increase in Si content of filler from 5 to 12% may not reduce the IMC layer thickness. Springer et al. [32] also reported thicker Fe_2Al_5 phase in diffusion studies of solid iron and molten Al–Si alloy and attributed it to temperature and time. It is noticed that the reaction layer of CMT [4043 (Fig. 4a–c) and 4047 (Fig. 5a–c)] and P-CMT [4043 (Fig. 4d–f)] joints is composed of two-layered IMC, i.e., white-coloured layer (L1) towards steel and light grey-coloured layer (L2) towards the bead throughout the cross section (head to foot). However, reaction layer of P-CMT (4047) (Fig. 5d–f) joints is comprised of three-layered IMC, i.e., white-coloured layer (L1) towards steel, dark grey-coloured layer (L2) and light grey-coloured layer (L3) towards the bead at centre (Fig. 5e), and two-layered IMC, i.e., white-coloured layer (L1) towards steel and light grey-coloured layer (L2) towards the bead at head (Fig. 9d) and foot (Fig. 9f) regions. It is also clearly evident that in all cases, irrespective of the filler wire used and location, L1 is thinner compared to the remaining layers. Jacome et al. [15] also reported thickening of IMC layer with increase in heat

input and multilayered reaction compound at bead/steel interface which is in agreement with the present observation.

It is also observed that bead/steel interface is comprised of two interfaces, i.e., (1) steel/IMC interface and (2) IMC/bead interface. Steel/IMC interface is found to be almost flat throughout the cross section in all cases. This is because, steel acts as a nucleation site for IMC to grow into the bead, but the IMC/bead interface morphology is found to vary with filler wire. In joints made using 4043 filler, the IMC/bead interface is wavy in nature with curved or rounded surface towards the bead (Fig. 4a–f). This type of morphology has also recorded delamination at IMC/bead interface, and the reason for this has been clearly explained in the subsequent sections. However, when joints are made using 4047 filler, the IMC/seam interface is an uneven blocky structure with flat surface towards bead. High diffusion rates in case of 4047 filler may result in variation in morphology.

3.4 Phase Analysis

Figures 6, 7, 8 and 9 depict the XRD patterns obtained from CMT and P-CMT weld-brazed joints made using 4043 and 4047 filler wires, at various locations (i.e., head, centre and foot). The composition of the phases derived from the XRD analysis is listed in Table 4. The XRD analysis of bead/steel interface of both CMT-4043 (Fig. 6) and P-CMT-4043 (Fig. 7) joints reveal the presence of two IMC phases, i.e., FeAl (cubic) and $Fe_{25}Al_{75}$ (monoclinic) throughout the cross section (head to foot). Therefore, the two intermetallic phases obtained from XRD pattern match with the two-layered reaction layer observed in respective

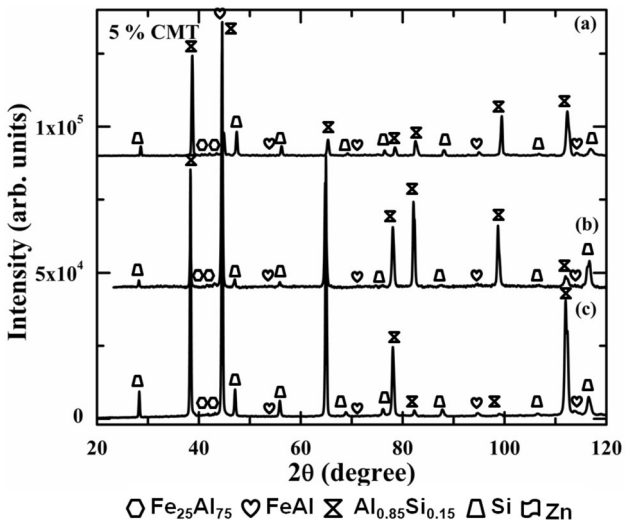

Fig. 6 XRD pattern obtained from various locations of seam/steel interface of CMT weld-brazed specimen made with Al–5%Si filler wire: **a** head, **b** centre, **c** foot

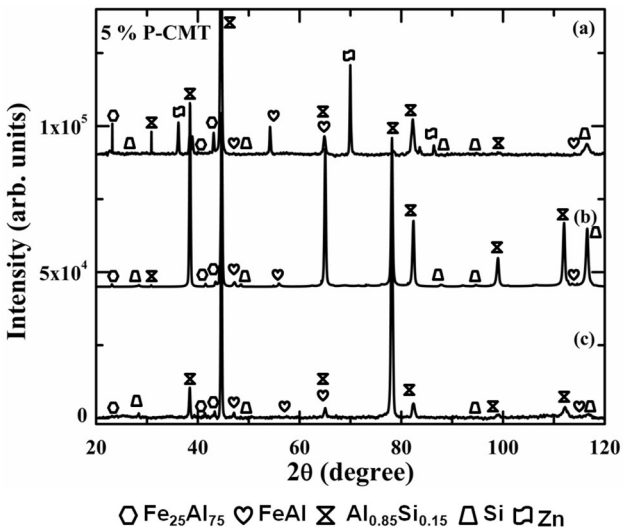

Fig. 7 XRD pattern obtained from various locations of seam/steel interface of P-CMT weld-brazed specimen made with Al–5%Si filler wire: **a** head, **b** centre, **c** foot

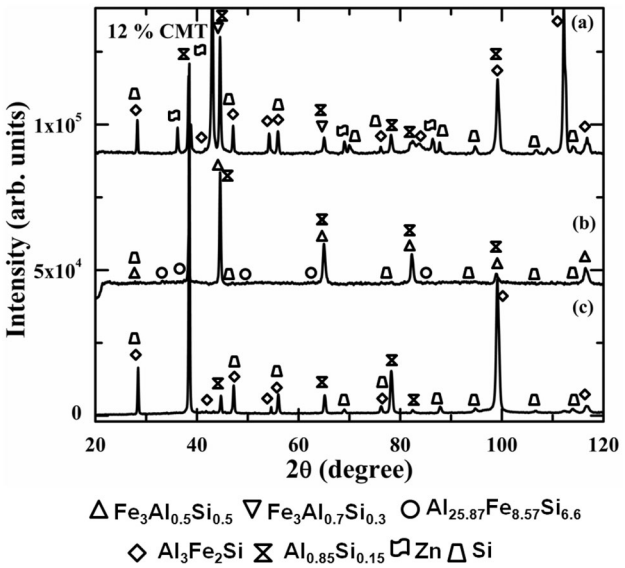

Fig. 8 XRD pattern obtained from various locations of seam/steel interface of CMT weld-brazed specimen made with Al–12%Si filler wire: **a** head, **b** centre, **c** foot

microstructures (Fig. 4). In general, layer towards the steel will be rich in Fe and layer towards the bead will be rich in Al [32]. Therefore, layer towards the steel (L1) may be FeAl; layer towards bead (L2) may be $Fe_{25}Al_{75}$ (Fig. 6a).

The XRD pattern obtained from bead/steel interface of CMT-4047 (Fig. 8) weld-brazed joint reveals the presence of two IMC phases, i.e., Fe-rich $Fe_3Al_{0.7}Si_{0.3}$ (cubic) and Al-rich Al_3Fe_2Si (cubic), at head and foot regions (Fig. 8) which agrees with their respective microstructures. As mentioned above, the Fe-rich $Fe_3Al_{0.7}Si_{0.3}$ (cubic) phase may be towards the steel side (L1) and Al-rich Al_3Fe_2Si

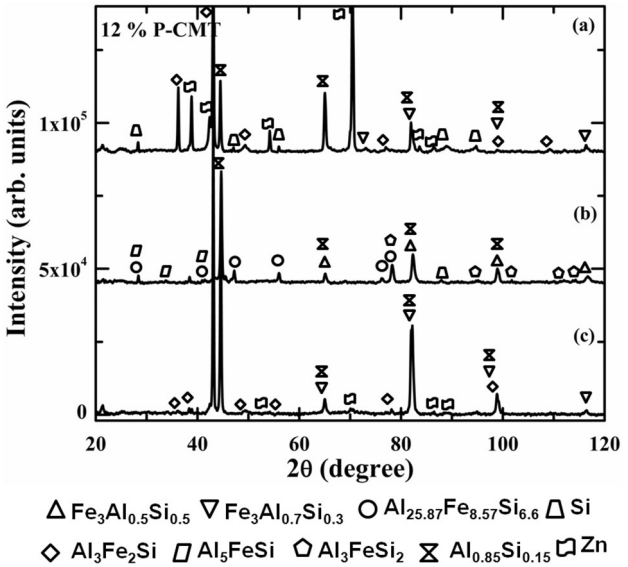

Fig. 9 XRD pattern obtained from various locations of seam/steel interface of P-CMT weld-brazed specimen made with Al–12%Si filler wire: **a** head, **b** centre, **c** foot

(cubic) may be towards the bead side (L2). Similarly, the central region is comprised of Fe-rich $Fe_3Al_{0.5}Si_{0.5}$(cubic) towards steel and $Fe_{8.57}Al_{25.83}Si_{6.6}$ (rhombohedral) IMC towards the bead (Fig. 5c). The phases $Fe_3Al_{0.7}Si_{0.3}$ and $Fe_3Al_{0.5}Si_{0.5}$ are the forms of Fe_3Al with varied Al/Si ratio. Al_3Fe_2Si and $Al_{25.83}Fe_{8.57}Si_{6.6}$ (approx Al_3FeSi) are phases with varied Al/Fe ratio. Varied diffusion rates governed by temperature variation at head, centre and foot regions may result in IMC phases with varied Al/Si and Al/Fe ratios.

The XRD pattern (Fig. 9) of P-CMT-4047 weld-brazed joints reveal the presence of two IMC phases, i.e. Fe-rich $Fe_3Al_{0.7}Si_{0.3}$ (cubic) towards steel and Al-rich Al_3Fe_2Si (cubic) towards the bead head (Fig. 9a) and foot region (Fig. 9c) which agrees with respective microstructures (Fig. 5d, f). It also reveals the presence of Fe-rich $Fe_3Al_{0.5}Si_{0.5}$ (cubic) towards the steel, medium Al-rich $Al_{25.83}Fe_{8.57}Si_{6.6}$ (rhombohedral) at middle and Al-rich Al_5FeSi (monoclinic) towards the bead with traces of Al_3FeSi_2 (tetragonal) at a central region (Fig. 9b) which agrees with respective microstructures (Fig. 5d). Al_3FeSi_2 (tetragonal) being a reaction product that is formed with Al_5FeSi in a Al–Fe–Si ternary system [33], is also observed. Therefore, joint made with 4043 and 4047 filler is comprised of binary (Fe–Al) and ternary (Fe–Al–Si) intermetallics, respectively. The phases like $Al_{0.85}Si_{0.15}$ (cubic), Zn (HCP), Si (cubic) are also observed which come from the bead.

3.5 Lap shear Test

The lap shear test has been performed on weld-brazed aluminium–steel joints, and its results are tabulated in Table 5. Mainly two types of failures are observed, i.e., interfacial failure and bead failure, as presented in Fig. 10. It is noticed that CMT joints show better fracture loads than P-CMT joints. High heat inputs compared to CMT involved in the P-CMT process, results in thicker IMC formation, thus recording lower fracture loads. It is observed that joints made using 4043 filler records low fracture loads (interfacial failure) than joints made using 4047 filler (bead failure) in all cases. Better wetting and spreading of 4047 filler on steel may probably result in high fracture loads. The strengths achieved in the present work are comparable with the reported values in the literature [5, 11].

Table 4 Composition of the intermetallic phases observed in XRD patterns

S. no	Phase	Composition (at.%)			Crystal structure
		Al	Fe	Si	
1	FeAl	50	50	–	Cubic
2	$Fe_{25}Al_{75}$	75	25	–	Monoclinic
3	Al_3Fe_2Si	50	333.33	16.67	Cubic
4	$Al_{25.83}Fe_{8.57}Si_{6.6}$	63	20.90	16.10	Rhombohedral
5	$Fe_3Al_{0.5}Si_{0.5}$	12.50	75	12.50	Cubic
6	$Fe_3Al_{0.7}Si_{0.3}$	17.50	75	7.50	Cubic
7	Al_5FeSi	71.43	14.29	14.29	Monoclinic
8	Al_3FeSi_2	50	16.67	33.33	Tetragonal

Table 5 Lap shear test results

S. no	Sample ID	Fracture load (N/mm) and failure location			
		Al–5%Si		Al–12%Si	
		CMT	P-CMT	CMT	P-CMT
1	S_1	236 (interface)	209 (interface)	250 (bead)	242 (bead)
2	S_2	232 (interface)	210 (interface)	260 (bead)	240 (bead)
3	S_3	233 (interface)	206 (interface)	257 (bead)	238 (bead)

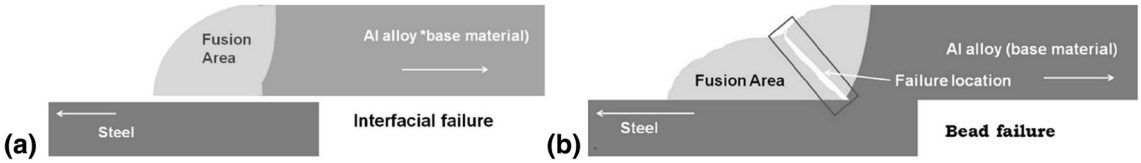

Fig. 10 Failure location in weld-brazed aluminium–steel joint: **a** interfacial failure, **b** braze bead failure

4 Discussion

4.1 Effect of interfacial morphology on failure

Figure 11 shows the high-magnification SEM images of bead/steel interfacial morphologies. The steel//IMC interface is almost flat in all cases. The layer adjacent to steel is found to be cubic throughout the cross section. Three types of IMC/bead interfacial morphologies like (1) wavy and curvy (Fig. 11a), (2) rectangular block (Fig. 11b), (3) irregular block with a flat surface (Fig. 11c) are observed.

Type 1 (wavy and curvy) morphology is evident in joints made with 4043 filler (CMT and P-CMT) (Figs. 4a–e and 11a). The interface is not flat, and delamination at IMC/bead interface is observed. The respective XRD analysis reveals the presence of binary $Fe_{25}Al_{75}$ (monoclinic) phase towards the bead. Therefore, incoherency between monoclinic-structured IMC and cubic-structured Al–Si bead may result in delamination at IMC/bead interface. Hence, in type 1 morphology, there are a strong steel/IMC interface and a weak IMC/bead interface. The samples possessing type 1 morphology (Figs. 4a–f and 11a) fails at IMC/bead interface recording the lowest fracture loads among the three types of interfacial morphologies.

The type 2 morphology is rectangular blocks (Figs. 5a–c and 11b) and is predominantly observed in CMT (4047) joints. The corresponding XRD analysis reveals the presence of Al_3Fe_2Si (cubic) phase towards the bead rendering the IMC/bead interface stronger without delamination. Hence, the interface is strong, and failure shifts to beads at higher fracture loads compared to other two interfacial morphologies as reported in lap shear test results (Table 5). Hence, having ternary IMC at Al//steel interface with crystal structures compatible with both steel and aluminium helps in strengthening the interface and maximizing the fracture load.

The type 3 morphology is irregular blocks with flat surfaces (Fig. 11c) and is likely to form at high heat input

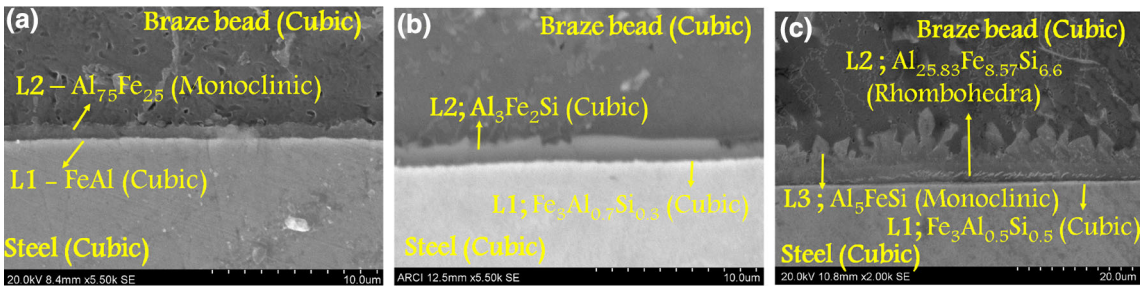

Fig. 11 Bead/steel interfacial morphology with probable IMC phases: **a** type I interface (wavy and curvy) CMT-5%Si and P-CMT-5%Si (head, centre, foot), **b** CMT-12%Si and P-CMT-12%Si (head and foot only), **c** type 3 interface (irregular blocks with flat edges) P-CMT-12%Si (centre only)

with 4047 filler. Among the three layers, layer 3 possesses the irregular block-shaped morphology with flat surfaces towards the bead (Figs. 5e and 11c). In this case, the interlock between layer 3 and seam is strong without any delamination. XRD analysis reveals that the layer towards the bead is Al_5FeSi (monoclinic) phase at centre and Al_3Fe_2Si (cubic) phase at head and foot regions. Therefore, in this case, also the steel/IMC interface and IMC/seam interface are strong, resulting in bead failure but at lower loads than type 2 morphology and higher than type 1 morphology. Therefore, types 2 and 3 morphologies avoid interfacial failures and among the two, type 2 morphology results in higher fracture loads. It is also observed that the presence of binary IMC phases is more detrimental compared to ternary IMC phases.

5 Conclusions

(1) The filler wire composition (Al–5%Si and Al–12%Si) and CMT modes (with and without pulsing) affected the nature of intermetallic compounds at Al/steel interface.

(2) Three types of IMC/bead interfacial morphologies were observed (a) type 1 (wavy and curvy); (b) Type 2 (rectangular block); and (c) type 3 (irregular blocks with a flat surface). Type 1 interfacial morphology was more prominently observed in joints made with 4043 filler. Types 2 and 3 interfacial morphologies were observed in joints made with 4047 filler wire. Type 2 morphology yielded the best strength among the three due to the favourable crystal structure of the IMC phases.

(3) The use of 4043 filler favoured the formation of Fe–Al-based binary IMC phases at the bead/steel interface; due to this, samples failed at the interfacial failure during lap shear test in the fracture load range of 208–233 N/mm.

(4) The use of 4047 filler favoured the formation of Al–Fe–Si-based ternary IMC phases at bead/steel interface and led to failure at bead during lap shear test in the fracture load range of 240–260 N/mm.

(5) Overall, the joints made with CMT process recorded superior properties than joints made with pulsed CMT process, and joints made with 4047 filler recorded higher fracture loads compared to joints made with 4043 filler.

Acknowledgements The authors are grateful for the financial support provided by the Technology Development Board (TDB), Department of Science and Technology, Government of India.

References

1. Ashby M F, *Materials selection in mechanical design*, Butterworth-Heinemann, Burlington, MA (2005).
2. Das A, Shome M, Goeck S F, De A, *J Manuf Process* **27** (2017) 179.
3. Song J L, Lin S B, Yang C L, Ma G C, Liu H, *Mater Sci Eng A* **509** (2009) 31.
4. Zhang H T, Feng J C, He P, *Mater Sci Technol* **24** (2008) 1346.
5. Zhang Y, Huang J, Cheng Z, Ye Z, Chi H, Peng L, Chen S, *Mater Lett* **172** (2016) 146.
6. Li L, Xia H, Tan C, Ma N, *J Mater Process Technol* **252** (2018) 573.
7. Sadeghian B, Taherizadeh A, Atapour M, *J Mater Process Technol* **259** (2018) 96.
8. Zhaoa D, Renb D, Zhao K, Pane S, Guo X, *J Manuf Process* **30** (2017) 63.
9. Mori K I, Abe Y, Int *J Lightweight Mater Manuf* **1** (2018)1.
10. Basak S, Das H, Pal T K, Shome M, *Mater Character* **112** (2016) 229.
11. Kreimeyer M, Sepold G, *in Proceedings of ICALEO* 2002.
12. Pang J, Hu S, Shen J, Wang P, Liang Y, *J Mater Process Technol* **238** (2016) 212.
13. Cao R, Huang Q, Chen J H, Wang P C, *J Alloys Compd* **585** (2014) 622.
14. Zhang H T, Feng J C, He O, Zhang B B, Chen J M, Wang L, *Mater Sci Eng A* **499** (2009) 111.
15. Jacome L A, Weber S, Leitner A, Aremholz E, Bruckner J, Hock H, Pyzalla A R, *Adv Eng Mater* **11** (2009) 350.
16. Yang J, Li Y, Zhang K, Guo W, *Mater Trans A* **46** (2015) 5149.
17. Krishna P Y, Ravi N B, Koteswararao V R, BhanuSankaraRao K, Padmanabham G, *J Mater Process Technol* **214** (2014) 2949.
18. Zhang H T, Liu J H, Feng J C, *Trans Nonferrous Met Soc China* **24** (2014) 2831.
19. Rong J, Kang Z, Chen S, Yang D, Huang J, Yang J, *Mater Charact* **132** (2017) 413.
20. Narsimhachary D, Pal S, Shariff S M, Padmanabham G, Basu A, *J Mater Eng Perform* **26** (2017) 4274.
21. Zhang Y, Guo G, Li F, Wang G, Wei H, *J Mater Process Technol* **246** (2017) 313.
22. Jia L, Shichun J, Yan S, Cong N, Junke C, Genzhe H, *J Mater Process Technol* **224** (2015) 49.
23. Qin G L, Su Y H, Wang S J, *Trans Nonferrous Met Soc China* **24** (2014) 989.
24. Murakami T, Nakata K, Tong H, Ushio M., *ISIJ Int* **43** (2003) 1596.
25. Ma H, Qin G, Ao Z, Wang L, *J Mater Process Technol* **252** (2018) 595.
26. Kang M, Kim C, *Mater Des* **81** (2015) 95.
27. Denner S G, Jones R D, *Met Technol* **4** (1977) 167.
28. Kobayashi S, Yakou T, *Mater Sci Eng A* **338** (2002) 44.
29. Chen N, Wang M, Wang H P, Wan Z, Carlson B E, *J Manuf Process* **34** (2018) 424.
30. Heumann T, Dittrich S, *Z Metall* **50** (1959) 617.
31. Eggeler G, Auer W, Kaesche H, *J Mater Sci* **21** (1986) 3348.
32. Springer H, Kostka A, Payton E J, Raabe D, Kaysser-Pyzalla K, Eggeler G, *Acta Mater* **59** (2011) 1586.
33. Raghavan V, *J Phase Equilib Diffus* **33** (2012) 322.